Reactivity of 1-Propanol on $p(n \times 2)$ Reconstructed $WO_3(100)$ Thin Films

M. Li,*,† W. Gao,† A. Posadas,‡ C. H. Ahn,‡ and E. I. Altman†

Department of Chemical Engineering, Yale University, New Haven, Connecticut 06520, and Department of Applied Physics, Yale University, New Haven, Connecticut 06520

Received: June 16, 2004; In Final Form: July 20, 2004

The reactivity of active sites on reduced $WO_3(100)$ thin film surfaces was studied using temperature-programmed desorption (TPD), Auger electron spectroscopy, low-energy electron diffraction, and scanning tunneling microscopy (STM). When films were annealed in either O_2 or NO_2 ($\sim 1 \times 10^{-6}$ Torr) above 700 K, the surfaces were predominantly covered by strands in a $p(n \times 2)$ periodicity with n ranging from 3 to 5. The catalytic activity of the $p(n \times 2)$ surfaces was probed using 1-propanol exposure at room temperature. During dosing, STM showed the accumulation of features associated with adsorption solely on the tops of the strands, unlike the stoichiometric $c(2 \times 2)$ $WO_3(001)$ surface which required annealing to desorb water before strongly localized features could be resolved. Thus the features in the images were attributed to 1-propoxide formed by deprotonation of the alcohol on adsorption at room temperature. High-resolution images revealed that the positions of the alkoxides on the strands were consistent with an added row model. Similar to other WO_3 surfaces, in TPD experiments only unreacted 1-propanol, water, and propene were observed, indicating that $p(n \times 2)$ surfaces are only active for dehydration. The propene, however, desorbed at much lower temperatures than from other WO_3 surfaces: around 400 K with much weaker peaks at 540 and 670 K. The 670 K desorption peak corresponded to that on other WO_3 surfaces and was attributed to desorption from a low coverage of higher oxygen concentration domains on the surface seen with STM. Thus the surface structure did not affect the reaction pathway but did affect the kinetics with the $p(n \times 2)$ strands active for dehydration of adsorbed alkoxides to form alkenes at much lower temperatures.

I. Introduction

Tungsten oxide thin films have been studied extensively due to their applications in gas sensing,[1,2] catalysis,[3,4] and electrochromic devices.[5,6] Supported tungsten oxides are used as catalysts for alkane isomerization,[7] alkene metathesis,[8,9] and partial oxidation reactions.[10] In addition, WO_3 is a key component in catalysts for the selective catalytic reduction of NO emitted from power plants by NH_3,[11] and it has been found that WO_3 supports can enhance the reactivity of Pt nanoparticles for the electro-oxidation of methanol in fuel cells.[12] Despite these diverse catalytic applications, the relationship between catalytic activity and function, such as dehydrogenation versus dehydration of alcohols, and catalyst structure still remains unclear for WO_3 specifically and more broadly for transition metal oxides (TMOs).

For TMOs, coordinatively unsaturated cation sites (cus's) have long been considered the active sites for catalytic reactions.[13] The catalytic activity of these sites depends on the oxidation state of the cus metal cation and can be structure-sensitive. It has been suggested that the structure sensitivity is related to different catalytic properties of neighboring bridging and terminal oxygen atoms, while others have argued that terminal oxygen atoms are not involved in catalytic reactions.[14,15] This motivated our previous study of the effects of cation oxidation state and terminal oxygen concentration on oxide catalysis using γ-$WO_3(001)$ single crystals where both parameters can be varied systematically.[16] The adsorption and reaction of alcohols were used as probe reactions because the reaction pathways for the alcohols are sensitive to the surface's redox and acid−base properties.[17] It was found that 5-fold coordinated W^{6+} cations act as alcohol dehydration sites on the fully oxidized (001)-oriented WO_3 surface. Subsequently, Ma et al. compared the interaction of alcohols with oxidized and reduced WO_3 thin films.[18,19] They found that while reducing the films made them more active for methanol deprotonation, the reduction did not substantially affect the behavior of higher alcohols. In their work, Ma et al. monitored the oxidation state of the surface W cations but did not characterize the surface structure. Tungsten oxide surfaces can display as many as seven different reconstructions as they are reduced. Thus, it is our current interest to extend our previous study to ordered, reduced (100)-oriented WO_3 thin films where the cus W^{5+} cation dominates and almost all terminal oxygens are removed.

The WO_3 bulk structure is constructed of corner-sharing WO_6 octahedra in a ReO_3-like framework; distortions and tilting of the octahedra lead to deviations from the ideal cubic structure.[20−24] Changes in the distortions result in a series of phase transitions. Between 290 and 630 K, monoclinic γ-WO_3 with lattice constants $a = 0.7297$ nm, $b = 0.7539$ nm, $c = 0.7688$ nm, and $\beta = 90.91°$ is favored; scanning tunneling microscopy (STM) experiments have been performed within this temperature range.[16,25,26]

It has been shown that $WO_3(001)$ single crystals display many surface reconstructions depending on treatment conditions. A $c(2 \times 2)$ structure[25,26] with half of the terminal oxygen atoms removed is considered "fully oxidized" since it is autocompensated with all W cations in the 6+ oxidation state. Reduction led to $p(2 \times 2)$,[25,26] $p(6 \times 2)$, and $c(4 \times 2)$[27] structures with

* Corresponding author. E-mail: min.li@yale.edu. Fax: +1 203-4324387.

† Department of Chemical Engineering.

‡ Department of Applied Physics.

10.1021/jp047383y CCC: $27.50
Published on Web 09/04/2004

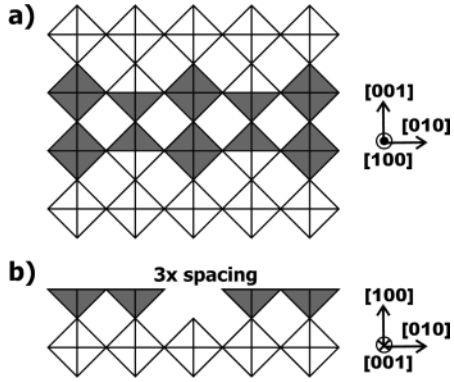

Figure 1. The added row model of $p(n \times 2)$ strands: (a) top view and (b) side view along a strand with 3× spacing. The dark octahedra represent W−O units in the strand.

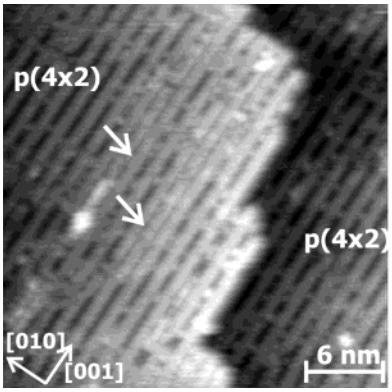

Figure 2. An STM image of the $p(n \times 2)$ surface obtained after annealing in NO_2 (1×10^{-6} Torr) at 710 K for 45 min. The arrows highlight local 3× spacing between strands.

1/4 monolayer (ML) of terminal oxygen and half of the exposed W cations reduced to 5+. Continued reduction ultimately produced a (1×1) surface with no terminal oxygen and all surface W cations reduced to 5+.[27] These structures were defined with respect to an idealized cubic unit cell with a lattice constant $l = 0.375$ nm; the same terminology will be used in this paper.

Despite a strong similarity between the WO_3 (100) and (001) planes, we recently found a series of $p(n \times 2)$ ($n = 3, 4, 5,$ etc.) surface reconstructions on (100)-oriented WO_3 epitaxial films that were not seen on (001)-oriented single-crystal surfaces.[28−30] The reconstructions were reproducibly created by reducing $p(2 \times 2)$ surfaces with progressive reduction decreasing n from 5 to 4 to 3; reducing the $p(3 \times 2)$ surface led to the (1×1) surface described above.[29] Our STM results showed that the $p(n \times 2)$ surfaces were covered by strands spaced nl ($n = 3, 4, 5,$ etc.) apart. The added row model pictured in Figure 1 was proposed for the strands.[28] The strands contain W and O atoms in gray octahedra located at their bulk (open octahedra) positions with all terminal oxygen removed from the top of the strand as seen along the strand in Figure 1b. Oxygen atoms are removed from the corner of every other octahedron creating local 2× periodicities along the [010] direction as shown from the top view of the surface in Figure 1a. While the stoichiometry of the top layer of the strand is WO_2, half of the oxygen atoms in the next layer down are associated with the strand giving an overall stoichiometry of W_2O_5, the same as the (1×1) surface; thus, all W cations on top of the strand are in the 5+ oxidation state. Oxygen atoms in the trough of Figure 1b lead to an overall O/W ratio slightly higher than that of the (1×1) surface, consistent with reduction decreasing the strand spacing and ultimately producing (1×1) terraces with no on-top oxygen.[29] The reliable recipe to prepare $p(n \times 2)$ surfaces amenable to STM imaging thus allows us to probe the role of the exposed cus cations with different oxidation states and coordination numbers in determining reaction pathways and kinetics in catalysis.

In this paper, we report on the catalytic properties of the $p(n \times 2)$ surface using 1-propanol as a probe molecule. It will be shown that the $p(n \times 2)$ surface exhibits only dehydration activity, that the propoxide intermediates bond to exposed W^{5+} cations on top of strands, and that the propoxide reacts to form propene at much lower temperatures than on other WO_3 surfaces.

II. Experimental Section

The (100)-oriented WO_3 films were grown on $LaAlO_3$(100) substrates using RF-magnetron sputtering with film thicknesses varying between 40 and 100 nm.[28] Surface characterization by STM, low-energy electron diffraction (LEED), Auger electron spectroscopy (AES), temperature-programmed desorption (TPD), and temperature-programmed mass spectrometry (TPMS) was performed in a separate ultrahigh-vacuum (UHV) system with a base pressure of 1×10^{-10} Torr. The temperature was measured by clamping a *K*-type thermocouple housed in a thin Ta tube against the sample surface.[31] The films were cleaned by annealing in NO_2 or O_2 ($\sim 1 \times 10^{-6}$ Torr) between 770 and 820 K until contaminants such as C and S were below the AES detection limit. Traces of potassium impurities were always detected with AES after the films were cleaned.

The STM measurements were performed after the sample was cooled to room temperature. Tungsten tips for STM were cleaned by electron beam bombardment prior to use. A tunneling current of 0.5 nA was used. Only empty state STM images corresponding to positive sample biases are presented in this paper as filled state imaging was not stable.

The (100)-oriented WO_3 epitaxial thin films could be repetitively oxidized and reduced to produce the strand-terminated $p(n \times 2)$ surfaces.[28] Figure 2 shows a terrace terminated by strands on the WO_3(100) surface after annealing in NO_2 (1×10^{-6} Torr) at 710 K for 45 min. A $p(4 \times 2)$ domain with 4× strand spacing can be seen on the upper and lower terraces, while strands 3× apart can also be seen as marked by the arrows. A low density of resolvable spots can be seen in the trough that might be due to impurities. The strands oriented along the [001] direction in Figure 2, while strands running in the orthogonal direction were found on different areas of the same surface. A staggered step runs across the image with a single-layer step height of 0.38 nm. Low-energy electron diffraction of such a surface yields a diffuse $p(3 \times 2)/p(2 \times 3)$ pattern[29] with a high background due to the mix of $p(4 \times 2)$ and $p(3 \times 2)$ domains. The epitaxial thin films were found to be much easier to reduce than WO_3(100) single crystals, as similar sample treatments produced the fully oxidized $c(2 \times 2)$ structure on the (001) surfaces of single crystals.[27,28]

The 1-propanol was purified using freeze−pump−thaw cycles until the gas line pressure did not rise above 5×10^{-4} Torr. The alcohol was dosed into the main chamber using two directed dosers that provide enhancement factors of roughly 5 and 45 over the background system pressure for exposure during in situ STM and TPD measurements, respectively. The 1-propanol dosing was performed at room temperature. A quadrupole mass spectrometer differentially pumped by a small ion pump and a nonevaporable getter pump was used for the TPD experiments. As described in section III, TPMS experiments were performed

after 1-propanol exposure in which full-range mass spectra were obtained while the sample temperature was ramped. This experiment identified the masses of the cracking fragments to be monitored in subsequent TPD experiments. Up to six masses were monitored during TPD where two fragments from the same molecule were monitored. The TPD curves presented in the paper are presented as the sum of two traces to improve the signal-to-noise ratio. The heating rate in the TPMS and TPD was set at 5 K/s. The contribution of alcohol adsorption on the sample holder can be neglected as a mica sample mounted the same way as the WO_3 samples showed no detectable 1-propanol or propene desorption following 1-propanol exposure.[16] However, depending on the background pressure of the UHV system, at high temperatures the contribution from the sample holder and adjacent areas to the water signal in TPD cannot be excluded.

III. Results

a. Temperature-Programmed Desorption. To probe the catalytic activity of WO_3(100) thin films, we chose to investigate the oxidative dehydrogenation versus dehydration behavior of adsorbed 1-propanol using TPD. A similar study was performed previously on the fully oxidized $c(2 \times 2)$ surface of (001)-oriented WO_3 single crystals using a series of alcohols: 1- and 2-propanol and 2-methyl-2-propanol (*tert*-butyl alcohol).[16] The only reaction products observed in TPD experiments were alkenes, the dehydration products. In moving from the tertiary to the secondary to the primary alcohol, the alkene desorption temperature increased, indicating that breaking the alcohol C−O bond was the rate-limiting step, a finding corroborated in a study of ethanol and 2-propanol adsorption on WO_3 thin films.[18] This paper focuses on how the surface chemistry changes when the surface is reduced to $p(n \times 2)$. The primary alcohol was studied because it is the most difficult to dehydrate and so a change in the surface's dehydration versus dehydrogenation activity would be most apparent. In addition, we previously found that the adsorbed alkoxide formed by deprotonating the alcohol was easiest to stabilize on WO_3(001) for imaging by STM because it exhibited the largest temperature difference between when the alcohol deprotonated and when the alkoxide reacted to form the alkene.[16]

To determine the desorption products from the reduced $p(n \times 2)$ surface, TPMS experiments in which full-range mass spectra were recorded as the sample temperature was ramped were performed initially. After a 338 langmuir 1-propanol dose at 310 K, a desorption peak at 360 K was observed for masses 58 and 31 amu. Meanwhile, masses 42, 41, 40, 39, 38, 27, 26, and 15 amu showed a strong peak at 360 K and much weaker peaks at 540 and 670 K. The product distribution did not change with exposure. Masses 58 and 31 amu correspond to C_3H_6O and CH_2OH, respectively, the predominant cracking fragments of 1-propanol. Mass 42 amu corresponds to C_3H_6 (propene), and all the other features can be assigned to cracking fragments of propene. Therefore, the desorption of unreacted propanol and the dehydration product propene were observed following 1-propanol adsorption on the reduced $p(n \times 2)$ surface. Thus for TPD experiments, masses 58 and 31 amu were monitored to detect unreacted 1-propanol, masses 42 and 39 amu were monitored to detect propene, and 18 amu was monitored to detect water. These masses were selected to provide the most intense signal while minimizing the overlap between fragments of 1-propanol and propene.

Figure 3 shows a series of TPD curves as a function of 1-propanol exposure. Before the TPD runs, the surfaces were imaged by STM and showed morphologies similar to that in Figure 2. Therefore, the TPD data predominantly reflect 1-propanol adsorption on a $p(n \times 2)$ surface with steps and troughs containing oxygen. Meanwhile, all terminal oxygens were removed from the strands yielding undercoordinated W^{5+} cations. At the lower dose of 135 langmuir, propene desorption was observed at 360 K. As the coverage was increased, unreacted 1-propanol was observed to desorb in a broad peak at a similar temperature. At the same time, small amounts of water were seen at 400 K. The increase in the water curve near the end of the TPD run may be due to degassing of the sample holder, although a similar increase was observed in prior TPD work on ethanol on a reduced WO_3 surface.[18] The ratio of unreacted propanol desorption versus propene increased with exposure, although it was difficult to determine the exact branching ratio because of differences in the sensitivity of the mass spectrometer to different species. The propene desorption temperature shifted slightly from 360 K at 135 langmuir to 370 K at saturation exposures above 270 langmuir.

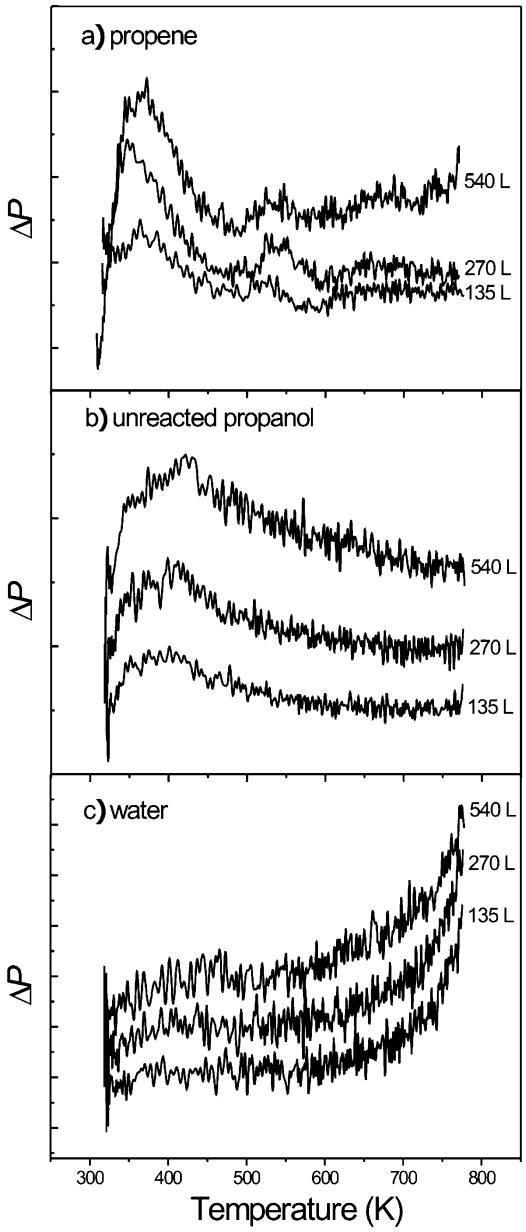

Figure 3. A series of TPD curves obtained as a function of 1-propanol exposure to the $p(n \times 2)$ WO_3(100) surface. The curves corresponding to different doses are offset along the pressure axis for clarity.

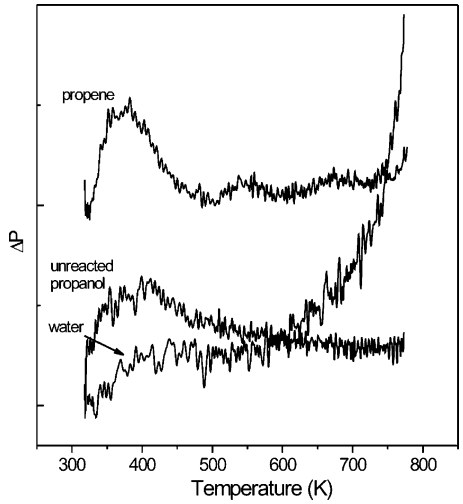

Figure 4. TPD curves for a saturation exposure of 540 langmuir of 1-propanol to the $p(n \times 2)$ surface.

The small peak shift with coverage suggests first-order desorption of propene on the $p(n \times 2)$ surface with adsorbates that weakly interact with one another. Therefore, similar to the $c(2 \times 2)$ surface of $WO_3(001)$ single crystals,[16] the propene desorption is dominated by the chemistry of individual sites even at saturation. Considering that 1-propanol dehydration yields one water molecule per propene molecule, the water desorption peaks were unexpectedly small. A couple of factors may explain this result. First, in the prior work on $c(2 \times 2)$ $WO_3(001)$ the alcohols were observed to dehydrate in two steps: (1) deprotonation of the alcohol to form an alkoxide and (2) C−O bond scission and β−H abstraction to form the alkene. During TPD experiments, two water desorption peaks corresponding to the two steps were observed, the first at about 400 K for 1-propanol. Based on STM results that showed the appearance of strongly localized features associated with adsorption only after annealing past this water desorption peak, the TPD peak was attributed to deprotonation of the alcohol to form a more strongly bound alkoxide and reaction of the liberated protons with surface O to form water. Following ethanol adsorption at 140 K on oxidized and reduced WO_3 films, Ma et al. observed water desorption peaks between 250 and 350 K depending on the ethanol coverage and state of the surface.[18] This suggests that 1-propanol deprotonates on the $p(n \times 2)$ surface at the 310 K adsorption temperature and half the water expected desorbs during adsorption by reaction of the protons with surface oxygen. The STM experiments described below support the formation of 1-propoxide near room temperature. In addition to water desorption during adsorption, WO_3 tends to intercalate H to form hydrogen tungsten bronzes,[32] and so some of the hydrogen may diffuse into the bulk rather than desorb as water over the temperature range studied.[16]

The observed dehydration temperature (360 K) of 1-propanol on the $p(n \times 2)$ surface is significantly lower than the 700 K observed on the fully oxidized $c(2 \times 2)$ surface.[16] This suggests that the C−O bonds become easier to break at W^{5+} sites on the strands. Meanwhile, the big downward temperature shift of water desorption from 700 K on the $c(2 \times 2)$ surface[16] to 400 K on the $p(n \times 2)$ surface suggests that the water desorption rate is largely governed by the rate of H abstraction from the alkoxide. This is consistent with a recent report that H diffusion on WO_3 surfaces is fast and that water desorbs from WO_3 below 300 K.[18]

Figure 4 shows the desorption traces from the $p(n \times 2)$ surface that were extracted from the saturation coverage in Figure 3. It can be seen that besides the major propene desorption peak at 360 K, there are also two small peaks at 540 and 670 K. The 670 K peak is in the temperature range where propene was observed to desorb from $c(2 \times 2)$ $WO_3(001)$ following 1-propanol adsorption[16] and where ethylene was observed to desorb from oxidized and reduced WO_3 thin films following adsorption of ethanol,[18] also a primary alcohol.

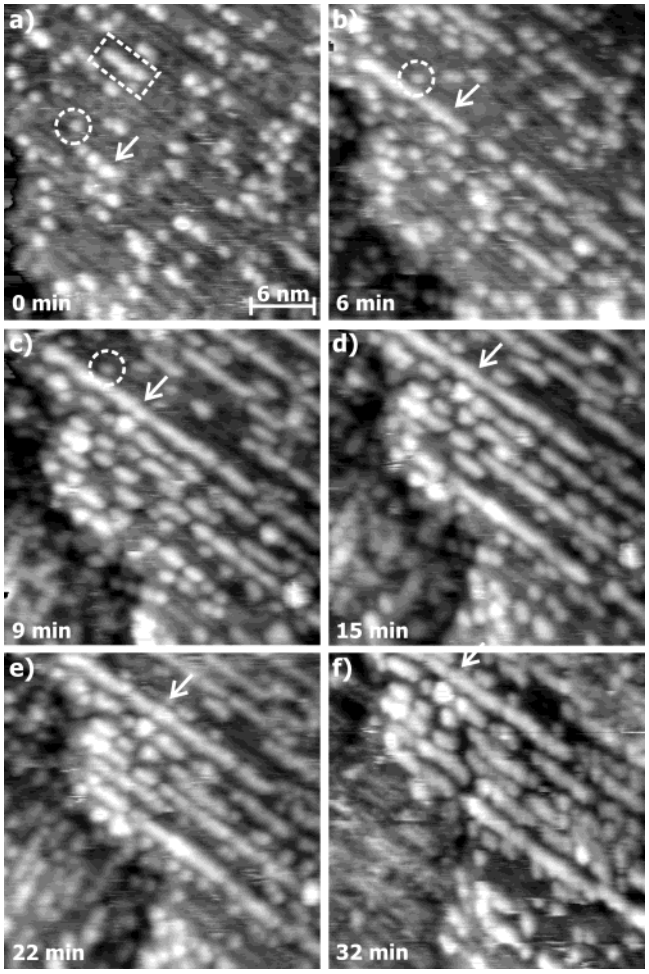

Figure 5. A sequence of STM images recorded during 1-propanol exposure to the $p(n \times 2)$ surface at 5×10^{-7} Torr and 300 K. The surface in image a was used as the starting point for the exposure time for images b−f. Prior to starting the sequence, the surface was exposed to 1-propanol, accounting for the white dots seen in image a. The sample biases were 2.25 V for image a, 2.55 V for images b−d, 2.5 V for image e, and 2.75 V for image f.

b. Scanning Tunneling Microscopy. Scanning tunneling microscopy was performed during 1-propanol exposure to determine the active sites for 1-propanol dehydration on the $p(n \times 2)$ surface. Before dosing, STM showed that the surface was terminated by strands similar to that in Figure 2. After a few minutes of 1-propanol dosing at room temperature, white spots began to appear on the surface as shown in Figure 5a. The strand structure can be resolved on the substrate, and scattered white spots accumulated exclusively on top of the strands. A few short chains formed by white spots on the strands can be seen in the box in Figure 5a. The image shows no preference for white spots to attach to the step. Using the time that Figure 5a was imaged as the starting point and continuing to dose for 6 more minutes, longer chains formed as indicated by an arrow in Figure 5b. The same site is highlighted by an arrow in all images in Figure 5. At 9 min, the strand indicated by the arrow in Figure 5b; was completely occupied by a long chain of adsorbates. Incoming propanol

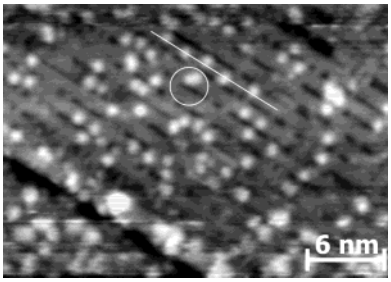

Figure 6. An STM image showing the surface after flashing to 420 K a $p(n \times 2)$ surface with a high density of adsorbates on the strands due to 1-propanol exposure. The line drawn through the center of the strand shows that the adsorbates locate off-center on top of the strands. The imaging bias was 2 V.

molecules tended to attach to existing longer chains, as some small spots, circled in Figure 5a−c, could still be seen after 9 min of exposure while a nearby strand was completely covered. As the exposure time increased above 9 min (Figure 5d,e) more long chains formed on the strands and no molecules were detected in the troughs, even after 32 min of 1-propanol exposure.

The images in Figure 5 show that features associated with 1-propanol adsorption can be readily imaged on the $p(n \times 2)$ surface following adsorption at room temperature. In contrast, on the WO_3(001) $c(2 \times 2)$ surface, such features were only observed after annealing the alcohol-covered surface above 400 K.[16] This observation was attributed to the deprotonation of molecularly adsorbed 1-propanol to form a more strongly bound alkoxide, consistent with water desorption observed in this temperature range. Thus the appearance of the stable white spots in the STM images of the $p(n \times 2)$ surface during dosing at room temperature and the unexpectedly small amount of water seen in the TPD experiments both support 1-propoxide formation at room temperature.

The TPD results suggest that 1-propanol dehydration on the $p(n \times 2)$ surface takes place mainly below 400 K, a much lower temperature than that at which primary alcohols dehydrate on other WO_3 surfaces.[16,18] Traces of dehydration products were also observed at 540 and 670 K, suggesting that dehydration may occur at multiple sites or that the low-temperature peak is anomalous. Therefore, to determine if the low-temperature dehydration is associated with adsorption on top of the strands, we dosed a $p(n \times 2)$ surface to a 1-propoxide coverage similar to that in Figure 5f and then heated the surface past the first propene desorption peak. After the surface was flashed to 420 K, the density of adsorbates on the strands decreased considerably as shown in Figure 6. Similar to the low 1-propanol exposures in Figure 5a,b, scattered white spots were observed exclusively on top of the strands. It can be seen that single adsorbates distribute off-center of the strand marked by a straight line. Occasionally, a cluster of two propoxide groups together could be resolved as shown in the circle. After further flashing to 570 K, past the second propene desorption peak at 540 K, none of the white spots remained on the strands, and the surface appeared similar to that in Figure 2. Thus we conclude that the strands are responsible for the observed low-temperature dehydration activity.

When surfaces such as those pictured in Figures 2, 5, and 6 were imaged over a wide range, structures corresponding to higher oxygen coverages were occasionally observed. In Figure 7, an island with a higher oxygen coverage can be seen surrounded by strands. The height between bright spots and vacancies on the island, 0.165 nm, and the appearance of these smaller, more discrete bright spots on the island are consistent

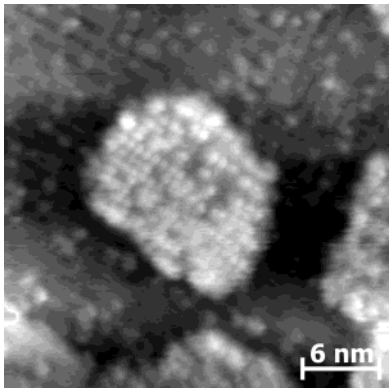

Figure 7. STM image of an island on the $p(n \times 2)$ surface obtained following a 180 langmuir 1-propanol dose at room temperature. The smaller, lower, or grayer dots on the island are assigned to terminal oxygen. The imaging bias was 2.25 V.

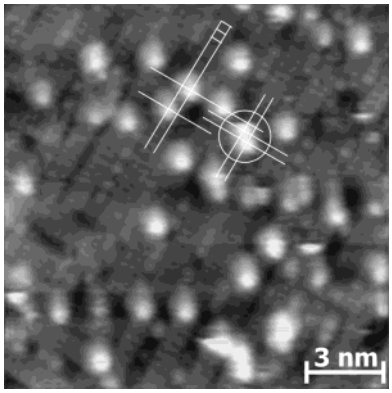

Figure 8. A high-resolution STM image obtained near the island in Figure 7. The image shows atomic resolution of the strands and the adsorbates which appear as diffuse white spots. The lines are drawn through the centers of the atoms on the strands to highlight the registry of the adsorbate features with the strands. The imaging bias was 2.75 V.

with terminal oxygen. The density of the spots is 1.43/nm^2, less than the 3.57/nm^2 for the stoichiometric $c(2 \times 2)$ surface; thus the island is reduced and exposes W^{5+} cations. The island and other structures like it can account for the weak propene desorption feature at 670 K. Again, alkene formation from primary alcohols was previously observed in this temperature range on $c(2 \times 2)$ WO_3(001) and oxidized and reduced WO_3 thin films.[16,19]

The deprotonation sites on top of the strands were resolved when a $p(n \times 2)$ surface was dosed with 180 langmuir of 1-propanol at room temperature. The high-resolution STM image in Figure 8 shows both the fuzzy white features associated with the adsorbates and the atomic-scale structure of the strands. In the image, the adsorbates locate off the center of the strands. Also on the tops of the strands, smaller protrusions in a (1×1) pattern can be seen. The grid superimposed on the image in Figure 8 shows that the adsorbates are centered on top of the protrusions that define the (1×1) pattern on the strands. As highlighted by the circle, the clusters composed of two adsorbates could be resolved as propoxide groups on opposite corners of the (1×1) unit cell. Features also appear in the troughs in Figure 8. The image in Figure 8 was recorded near the oxygen-rich island in Figure 7; there were also other oxygen-rich terraces nearby. Since similar features were not seen in numerous other images, see Figure 6 for example, the appearance of the trough in Figure 8 was attributed to defects

associated with an increased oxygen concentration rather than adsorption into the trough.

It has been shown that exposed cus W cations are the adsorption sites for alkoxides created by deprotonating alcohols.[16] This suggests that the protrusions forming the (1 × 1) pattern on the strand correspond to cus W cations. This supports the added row model presented in Figure 1 since it places exposed W cations spaced 1× apart along and across the strands. All of the terminal O is removed from the strands, leaving only coplanar W and O ions. In this case, only the W ions are resolved in empty state STM images since the density of unoccupied states just above the conduction band edge is concentrated around the W ions.[25,26] These data taken together all support the added row model.

It is also interesting that neighboring adsorbates tend to occupy opposite sides of the strands as shown in the circles in Figures 6 and 8. In the added row model, half of the oxygen is removed from the sides of the strands to maintain the same stoichiometry as larger (1 × 1) terraces. This constraint was adopted because during reduction the $p(n \times 2)$ structures were seen prior to the (1 × 1) structure. In Figure 1, the oxygen atoms are removed from both sides of the strand in a 2× periodicity along the strand. A zigzag pattern, however, would give the same stoichiometry. This suggests that differences in the reactivity between 4- and 5-fold coordinated W ions could cause neighboring adsorbates to occupy alternate sides of the strands. The zigzag pattern, however, is not consistent with bias-dependent imaging that showed a transition from a 1× periodicity along the strand to a 2× periodicity at higher biases.[28] The 2× periodicity was attributed to the missing O atoms on the sides of the strands and is not consistent with a zigzag model.[28] Therefore, the tendency of neighboring adsorbates to occupy opposite sides of the strands is attributed to adsorbed propoxide inhibiting adsorption and deprotonation at nearest neighbor sites rather than a difference in reactivity between 4- and 5-fold coordinated W ions.

IV. Discussion

The observation of propene and water as the only reaction products following 1-propanol adsorption indicates that the stranded $p(n \times 2)$ surface is active for dehydration but not oxidative dehydrogenation. Stoichiometric $c(2 \times 2)$ $WO_3(001)$ single crystals and oxidized and reduced WO_3 thin films were also observed to produce only dehydration products following adsorption of primary, secondary, and tertiary alcohols.[16,19] Thus the WO_3 surface structure and surface oxidation state do not affect the surface's relative dehydration versus dehydrogenation activity. On the other hand, propene evolves from the stranded surface at much lower temperatures than from the other WO_3 surfaces. Since alkene desorption from the other WO_3 surfaces has been shown to be reaction-rate-limited,[16,19] this indicates that the stranded surface is much more active for dehydration.

To understand why the surface structure and oxidation state do not affect the reaction pathway but do affect the reactivity, the reaction mechanism must be considered. The reactions of alcohols with oxide surfaces are generally considered to proceed through two steps: (1) deprotonation of the alcohol to form an alkoxide and either (2a) C−O bond scission and β−H abstraction of the alkoxide to form the alkene or (2b) α−H abstraction of the alkoxide to form an aldehyde or ketone.[17,33] The first step proceeds on Lewis acid−base pairs formed by a cus metal cation and a neighboring O atom, with the alkoxide binding to the acidic metal cation and the hydrogen to the basic O atom. On WO_3 at room temperature, the hydrogens can rapidly diffuse and combine to form water which then desorbs.[19] Whether the remaining alkoxide then reacts to form the alkene or carbonyl depends on the acidity of the metal cation and the basicity of the neighboring O atom or, phrased another way, the strength of the metal−alkoxide bond and the ability of the O to abstract a H atom. The appearance of only the dehydration products for WO_3 suggests that the exposed W cations are acidic while the neighboring O atoms are only weakly basic, in keeping with catalytic studies that classify tungsten oxides as acidic.[34] This is supported by comparisons of the behavior of primary, secondary, and tertiary alcohols on WO_3 that indicate that C−O bond scission is the rate-limiting step in the dehydration of the alkoxide and thus that the surface O atoms are poor at abstracting H atoms.[16] The lack of any change in the reaction products when the WO_3 surface is oxidized and reduced indicates that the balance between the acidity of the cus W cation and the basicity of the neighboring O atom is not substantially altered by oxidation and reduction, at least when reduction is limited to creating only W^{5+}. Further, the reaction mechanism suggests that alkoxides adsorbed on the strands dehydrate at lower temperatures because of a stronger W−O bond and consequently weaker C−O bond in the adsorbed complex. Although a shift in the rate-limiting step to H abstraction on the stranded surface cannot be ruled out, unless the C−O bond is also substantially weakened such a large increase in the ability of the surface to abstract H would shift the desorption product to the aldehyde, which was not observed.

In prior work on the effect of reduction of (001)-oriented WO_3 thin films on alcohol adsorption and reaction, Ma and Frederick did not see a large change in alkene desorption temperatures.[19] As reviewed in the Introduction, WO_3 displays a number of surface phases as it is reduced. In their work, Ma and Frederick did not characterize the structure of their reduced surfaces, and thus it is likely their surfaces were different from the stranded $p(n \times 2)$ surface focused on here. Still, all the ordered reduced WO_3 surfaces expose W^{5+}, suggesting that the structure of the strands and not the oxidation state of the exposed W cations prior to adsorption is responsible for the low-temperature alkoxide dehydration. In looking at Figure 1, the strands have a couple of unique features that could be responsible for their distinct behavior. The strands expose 4-fold coordinated W^{5+} cations, while only 5-fold coordinated W is exposed on the terraces of the other ordered structures. While the sides of the strands appear similar to monatomic steps on the (1 × 1) surface, STM images of (1 × 1) surfaces reveal predominantly fractional height steps due to shear planes intersecting the surface that do not expose 4-fold coordinated W^{5+}. A stronger adsorbate bonding to 4-fold coordinated W^{5+} would be expected and could explain the lower temperature dehydration activity. The model in Figure 1, however, suggests that stronger bonding to the 4-fold sites would lead to a 2× periodicity of propoxides along the strands, which was not observed.

Alternatively, the narrowness and corrugation of the strands could affect reactivity. As noted above, at room temperature on WO_3 the hydrogens liberated by alcohol deprotonation rapidly diffuse and combine to form water; desorption of the water reduces the surface. The terminal O in the trough would appear to be the logical one to remove in this process; however, Figure 1b shows that this would require the H to jump an unrealistically large distance and so the H may be restricted to stay on the same strand as the alkoxide. Removing additional oxygen from the strand would create 4-fold coordinated W^{4+} which would be expected to form a very strong W−O bond in

the adsorbed complex. Breaking the resulting weak C−O bond would restore the oxidation state to W^{5+}. Since both the deprotonation step and the C−O bond breaking step produce one water molecule for every two alcohol molecules, the overall reaction neither oxidizes nor reduces the surface. Compared to the (1 × 1) surface, the narrow width of the strands restricts the location of the more deeply reduced sites to the vicinity of the alkoxide. Preferential adsorption at these reduced sites could explain the observed growth of chains of adsorbates covering entire strands while neighboring strands were empty. A difficulty with this explanation is that the STM images show no obvious indication of reduction to W^{4+} which, because of electronic differences, should be distinguishable from W^{5+}.

V. Summary

The adsorption and reaction of 1-propanol on strand-terminated $p(n \times 2)$ WO_3(100) surfaces were characterized using TPD and STM. All the terminal oxygens are removed from the strands leaving W^{5+} cations on top of the strands. These cus W^{5+} cations provide acidic sites for 1-propanol adsorption via deprotonation to form 1-propoxide groups at room temperature, which then convert to propene upon heating. Similar to other WO_3 surfaces, no evidence of dehydrogenation products was observed; thus changing the structure and the oxidation state of the exposed W cations from 6+ to 5+ does not change the favored reaction pathway. On the stranded surface, however, the dehydration reaction proceeded at much lower temperatures, indicating that the surface structure can strongly affect the kinetics. Scanning tunneling microscopy showed that the 1-propoxide groups adsorb exclusively on top of the strands without an obvious preference for 4- or 5-fold coordinated cus W cations. High-resolution images showed that the propoxide groups locate directly above bright spots on the strands, supporting an added row model of the strands. The low-temperature dehydration activity of the strands was attributed to a stronger W−O bond in the adsorbed 1-propoxide that facilitates initiating the reaction at lower temperature by breaking the resulting weaker C−O bond.

Acknowledgment. The authors acknowledge the help of Jun Wang in carrying out this work. A. Posadas and C. H. Ahn acknowledge support from the National Science Foundation (DMR-0134721). This project is supported by the Department of Energy through Basic Energy Sciences Grant Number DE-FG02-98ER14882.

References and Notes

(1) Lee, D.-S.; Nam, K.-H.; Lee, D.-D. *Thin Solid Films* **2000**, *375*, 142−146.

(2) Kawasaki, H.; Namba, J.; Iwatsuji, K.; Suda, Y.; Wada, K.; Ebihara, K.; Ohshima, T. *Appl. Surf. Sci.* **2002**, *197*−*198*, 547−551.

(3) Gutiérrez-Alejandre, A.; Ramírez, J.; Busca, G. *Catal. Lett.* **1998**, *56*, 29−33.

(4) Wang, Y.; Chen, Q.; Yang, W.; Xie, Z.; Xu, W.; Huang, D. *Appl. Catal., A* **2003**, *250*, 25−37.

(5) Bessiere, A.; Marcel, C.; Morcrette, M.; Tarascon, J. M.; Lucas, V.; Viana, B.; Baffier, N. *J. Appl. Phys.* **2002**, *91*, 1589−1594.

(6) Fang, G.; Li, D.; Yao, B. *J. Phys. D*: *Appl. Phys.* **2001**, *34*, 2260−2266.

(7) Ono, Y. *Catal.Today* **2003**, *81*, 3−16.

(8) Verpoort, F.; Fiermans, L.; Bossuyt, A. R.; Verdonck, L. *J. Mol. Catal.* **1994**, *90*, 43−52.

(9) Yoshinaga, Y.; Kudo, M.; Hasegawa, S.; Okuhara, T. *Appl. Surf. Sci.* **1997**, *121*−*122*, 339−342.

(10) Xia, X.; Jin, R.; He, Y.; Deng, J.; Li, H. *Appl. Surf. Sci.* **2000**, *165*, 255−259.

(11) Amiridis, M. D.; Solar, J. P. *Ind. Eng. Chem. Res.* **1996**, *35*, 978.

(12) Park, K.; Ahn, K.; Nah, Y.; Choi, J.; Sung, Y. *J. Phys. Chem. B* **2003**, *107*, 4352−4355.

(13) Burwell, R. L.; Haller, G. L.; Taylor, K. C.; Read, J. F. *Adv. Catal.* **1969**, *20*, 1−96.

(14) Hermann, K.; Witko, M.; Druzinic, R. *Faraday Discuss.* **1999**, *114*, 53−66.

(15) Friend, C. M.; Queeney, K. T.; Chen, D. A. *Appl. Surf. Sci.* **1999**, *142*, 99−105.

(16) Tanner, R. E.; Meethunkij, P.; Altman, E. I. *J. Phys. Chem. B* **2000**, *104*, 12315.

(17) Tatibouët, J. M. *Appl. Catal., A* **1997**, *148*, 213.

(18) Ma, S.; Frederick, B. G. *J. Phys. Chem. B* **2003**, *107*, 11960−11969.

(19) Ma, S.; Amar, F. G.; Frederick, B. G. *J. Phys. Chem. B* **2003**, *107*, 1413−1423.

(20) Salje, E. *Acta Crystallogr.* **1977**, *B33*, 574−577.

(21) Salje, E.; Viswanathan, K. *Acta Crystallogr.* **1975**, *A31*, 356−359.

(22) Salje, E.; Rehmann, S.; Pobell, F.; Morris, D.; Knight, K. S.; Herrmannsdörfer, T.; Dove, T. *J. Phys. C*: *Solid State Phys.* **1997**, *9*, 6563.

(23) Loopstra, B. O.; Boldrini, P. *Acta Crystallogr.* **1966**, *21*, 158−162.

(24) Diehl, R.; Brandt, G. *Acta Crystallogr.* **1978**, *B34*, 1105−1111.

(25) Jones, F. H.; Rawlings, K.; Foord, J. S.; Cox, P. A.; Egdell, R. G.; Pethica, J. B.; Wanklyn, B. M. R. *Phys. Rev. B* **1995**, *52*, 14392.

(26) Jones, F. H.; Rawlings, K.; Foord, J. S.; Egdell, R. G.; Pethica, J. B.; Wanklyn, B. M. R.; Parker, S. C.; Oliver, P. M. *Surf. Sci.* **1996**, *359*, 107−121.

(27) Tanner, R. E.; Altman, E. I. *J. Vac. Sci. Technol.* **2001**, *A19*, 1502−1509.

(28) Li, M.; Altman, E. I.; Posadas, A.; Ahn, C. H. *Surf. Sci.* **2003**, *542*, 22−32.

(29) Li, M.; Altman, E. I.; Posadas, A.; Ahn, C. H. *Thin Solid Films* **2003**, *446*, 238−247.

(30) Li, M.; Altman, E. I.; Posadas, A.; Ahn, C. H. *J. Vac. Sci. Technol., A* **2004**, *22*, 1682−1690.

(31) Nakakura, C. Y.; Phanse, V. M.; Zheng, G.; Bannon, G.; Altman, E. I.; Lee, K. P. *Rev. Sci. Instrum.* **1998**, *69*, 3251.

(32) Hurditch, R. *Electron. Lett.* **1975**, *11*, 142.

(33) Farneth, W. E.; McCarron, E. M., III; Sleight, A. W.; Staley, R. H. *Langmuir* **1987**, *3*, 217−223.

(34) Kulkarni, D.; Wachs, I. E. *Appl. Catal., A* **2002**, *237*, 121.